Back Analysis of a Landslide in a Residual Soil Slope in Rio de Janeiro, Brazil

Denise Maria Soares Gerscovich, Eurípedes do Amaral Vargas Jr., Tacio Mauro Pereira de Campos

Abstract. After a short period of relatively intense rainfall, a deep-seated landslide occurred in a slope in Rio de Janeiro. On the following day, field inspection revealed full saturation of the failure mass, despite the inexistence of groundwater in the slope. A comprehensive experimental investigation was undertaken to determine the geotechnical parameters of the residual soil. A numerical modeling study of the infiltration processes revealed that the rainfall amount was insufficient to reproduce the saturation condition of the failure surface. This paper introduces the slope stability approach aiming to verify if the factor of safety would reflect a stable condition under the pluviometric records that occurred before the landslide. Therefore, 2D limit equilibrium analyses were accomplished, considering the different hydrological scenarios that were conceived for the flow simulations. The geotechnical parameters were defined according to laboratory test carried out on samples extracted from the slide surface and from an undisturbed site. Pore pressure distributions were obtained from previous results of flow simulations. Regardless of the geometry of the failed mass, the analyses indicated that the landslide could not be triggered solely by rain infiltration. Amongst various alternatives, a preferential flow through the bedrock fractured layer revealed to be the only feasible scenario that could reproduce not only the saturated condition, but also a FS value close to 1. Despite the usual approach of identifying the landslide as a rainstorm-induced mechanism, it appears to be more complex and other infiltration sources may play an essential role.

Keywords: unsaturated soil, residual soil, transient flow, rainfall, stability analysis, landslide.

1. Introduction

Rio de Janeiro city is located in the southeastern region of Brazil. Its mountainous landscape associated to a tropical humid climate results in slopes of unsaturated residual soil with thickness that may vary from a few centimeters to dozen of meters. Rain-induced soil and/or rock mass movements are quite frequent, during or immediately after periods of intense rainfall.

Despite the considerable progress in the understanding of the behavior of unsaturated soils, it is actually very difficult to predict when or where a landslide may happen. Nevertheless, it is recognized that rainfall-induced landslides are caused by changes in pore water pressures.

Many authors have attempted to address the probable causes of landslides (*e.g.* Kim *et al.*, 2004; Capra *et al.*, 2003; Gasmo *et al.*, 2000; Au, 1998; Costa Nunes *et al.*, 1989; Wolle & Hachich, 1989; Vargas *et al.*, 1986). Shallow failures may be attributed to the deepening of a wetting front into the slope, which results in a decrease of matric suction or to the development of the weathering process of steep slopes. Large landslides and debris flows usually result from the development of positive pore pressures that comes along with fully saturation of the soil mass. This scenario may be achieved when infiltrating water encounters a low permeability soil layer and a transient perched water table occurs (Capra *et al.*, 2003) or when water infiltrates through fractured layers of the bedrock (Dietrich *et al.*, 1986; Wilson, 1988; Vargas Jr. *et al.*, 1990). Further studies have also illustrated that positive pore pressure generation along the failure surface may be produced by the crushing of soil grains resulting in a liquefied soil condition (Wang & Sassa, 2003) or as a consequence of soil contraction that originates at the sliding surface and spreads to the unsaturated soil mass (Capra *et al.*, 2003).

In February 1988, a considerable number of soil/rock slides occurred in various slopes in Rio de Janeiro city. Most of them were shallow and quite long in extension (100-150 m) and were classified as being amongst the largest that have occurred in the city. The pluviometric data corresponding to 21 days indicated an accumulated amount of 515.6 mm, with a rain peak of 85.4 mm in a single day.

Nine months later, in November, a deep-seated slide occurred in a re-vegetated slope (Fig. 1) after a period of a medium intensity rainfall. After 21 days, the accumulated rainfall amount was 246.3 mm, with a maximum rain peak of 57.5 mm (Fig. 2). The failure caused structural and material damages to an adjacent building, with the shearing of one pillar and complete destruction of one apartment. Sev-

Denise Maria Soares Gerscovich, Departamento de Estruturas e Fundações Universidade do Estado do Rio de Janeiro, Rio de Janeiro, RJ, Brazil. e-mail: deniseg@uerj.br.
Eurípedes do Amaral Vargas Jr., Departamento de Engenharia Civil, Pontifícia Pontifícia Universidade Católica do Rio de Janeiro, Rio de Janeiro, RJ, Brazil. e-mail: vargas@civ.puc-rio.br.
Tacio Mauro Pereira de Campos, Departamento de Engenharia Civil, Pontifícia Universidade Católica do Rio de Janeiro, Rio de Janeiro, RJ, Brazil. e-mail: tacio@civ.puc-rio.br.
Submitted on July 15, 2010; Final Acceptance on January 11, 2011; Discussion open until December 30, 2011.

Figure 1 - Slope view on the day after.

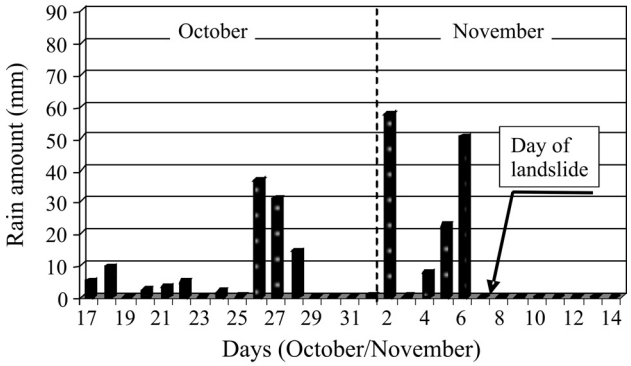

Figure 2 - Daily pluviometric data.

eral cars in external and internal building parking areas were also damaged. Fortunately, nobody was injured. Despite no evidence of groundwater within the slope, on the following day and continuously for the following week after the slide, there were clear indications of full saturation of the failure surface, with groundwater springs in its upper region.

Figure 3 shows a schematic topographic plan of the site before the landslide. The slope crest has a maximum elevation of 384 m and surface inclinations ranging from 30° to 55°. At the toe of the slope there was a gravity wall aligned with an anchored wall, located at the rear of Building A. The superficial drainage system, located in the upper region of the slope, was presumably malfunctioning, since blockage of the channel adjacent to the slide was observed during field inspections.

Preliminary analyses disregarded the hypothesis of failure of the retaining wall structure as the shape of the failure surface suggested a major tendency of soil movement over the wall crest. There was also no evidence that the accumulated rainfall could have raised the water table, which was located at a considerable depth below ground level. Using a simple one-dimensional water balance, one can prove that a large amount of water would be required to achieve soil saturation. Considering, for example, the average depth of the sliding mass to be approximately 5 m, fully drained condition and typical values of porosity ($n = 0.38$) and volumetric water content ($\theta = V_w/V = 0.1$), then the difference between both parameters gives the available volume of voids to be filled. Therefore, full saturation of the profile would require at least 1400 mm of infiltrating water. Besides this unrealistic value, the actual volume of water that infiltrates, compared to the rainfall rate, depends, among other factors, on the initial soil moisture condition, slope angle, vegetation type, etc. Consequently, the amount of infiltration would be less than the values predicted by the pluviometers data. Nevertheless, the triggering mechanism was undoubtedly associated to changes in the pore water

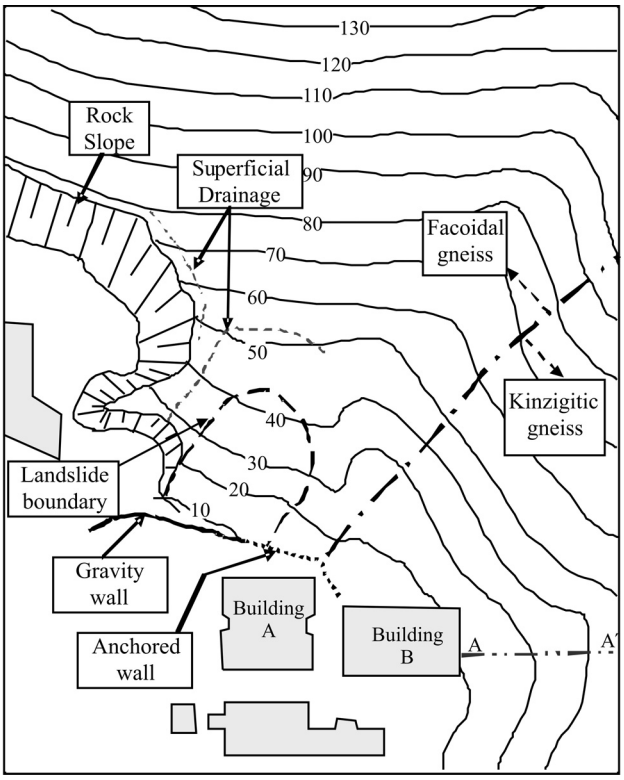

Figure 3 - Schematic site plan before landslide.

pressure and it was likely that complex changes of the slope hydrogeology might have occurred.

Numerical 3D-FEM transient flow analyses were carried out to identify the infiltration process that could explain field evidence of complete saturation of the failure surface. Different boundary conditions were conceived and the results revealed that only major changes of the slope hydrogeology could justify the deep-seated slope failure (Gerscovich *et al.*, 2006).

This paper describes the investigations that were carried out after the slope failure in order to define soil stratigrafy and the geotechnical parameters of the residual soils. Slope stability analyses were also performed with pore water meshes previously obtained from transient flow simulations.

2. Geotechnical Investigation

A comprehensive series of field and laboratory tests was carried out to determine soil profile and geotechnical and hydrological parameters. Field investigation comprised seismic refraction surveys, percussion and rotary drillings. Twenty-one holes were drilled for the installation of fifteen piezometers and six slope indicators, outside the slide area. Maxima piezometers (Brand, 1985) were also installed at the soil-rock interface to record maximum transient water pressure levels A pluviometric station was installed on the roof of the building, as well. For more details regarding field instrumentation refer to Gerscovich *et al.* (2006).

The soil profile showed depths varying from 0 to 15 m and was originated from a gneissic metamorphic rock that outcropped at the upper and left sides of the landslide boundary. The weathering profile was composed of a superficial mature clayey sand residual soil, with an average thickness of 1 m, underlain by a layer of a sandy matrix young residual soil (saprolitic soil), with a well defined inherited mineral alignment from the parent rock. The transition between the sound rock and the saprolitic soil is a highly fractured and weathered rock with a thickness varying within 4 m to 10 m. The mechanical soundings did not indicate the presence of a groundwater level within the soil mass. However, water level was observed in some rotary drillings within the fractured rock layer. Figure 4 illustrates the a cross section of the slope behind building B (section AA' - see Fig. 3).

Topographic plans that were generated before and after the slide, aero photos taken between 1966 and 1975, and logging profiles were used to restore the original geometry of the whole area as well as to define the landslide surface. The failure surface presented an ellipse shape with the relationship width (perpendicular to the movement) and length (along the direction of the movement) of approximately 0.6. Figure 5 displays the reconstructed 2D central section of the slope and the 3D geometry along with boundaries description.

Block samples were extracted from the slope failure surface and from a trench located 50 m away from the failure zone. The laboratory investigation comprised geotechnical characterization, determination of hydraulic parameters (hydraulic conductivity and water retention curve) and shear strength tests.

2.1. Soil characterization

Table 1 shows a summary of the characterization tests with the average physical indexes. Two different materials appeared at the failure surface: an apparently homogeneous and isotropic red-colored mature residual soil, and a grey saprolitic soil, with a well-defined mineral alignment. At the trench, only the saprolitic soil was extracted and it was coarser and denser than the one from the slip surface.

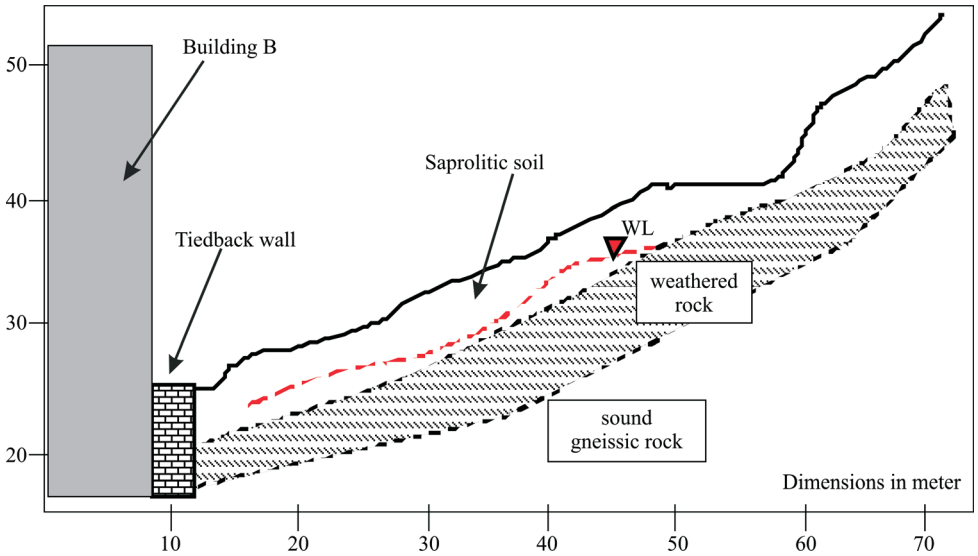

Figure 4 - Cross section behind building B.

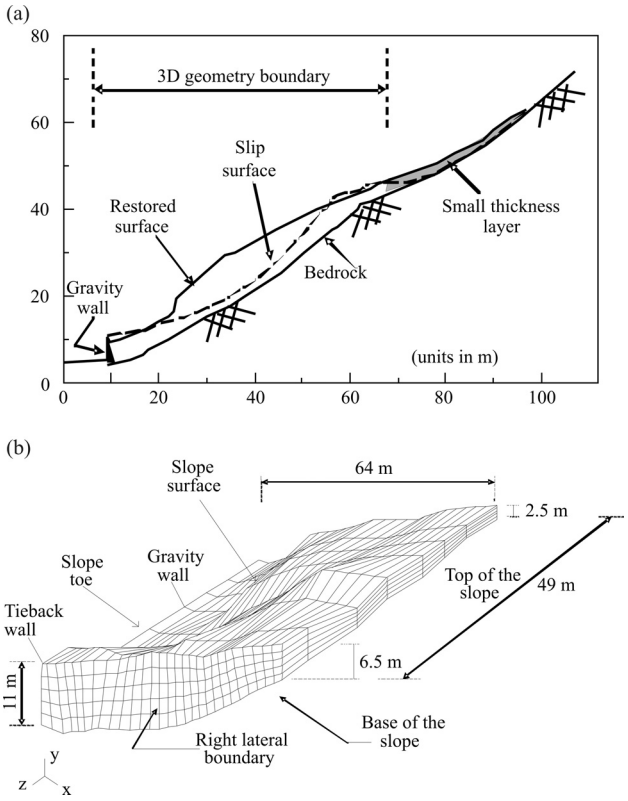

Figure 5 - Restored geometry. (a) Central section of the slope. (b) 3D geometry and boundaries description.

Table 1 - Soil characterization.

Location	Slip surface		Trench
Soil type	Saprolitic soil	Mature soil	Saprolitic soil
Sand (%)	63.0	56.0	82.0
Silt (%)	27.5	34.0	9.8
Clay (%)	9.5	10.0	8.2
ω_L (%)	38.2	39.5	-
ω_P (%)	NP	24.7	-
ω (%)	19.0	21.2	6.4
θ (%)	22.4	25.5	10.3
G_s	2.64	2.63	2.66
e	1.19	1.14	0.62
n	0.54	0.53	0.38
γ_t (kN/m^3)	14.0	14.6	17.1

Notes: ω_L = liquid limit, ω_L = plasticity limit; ω = water content; θ = volumetric water content; G_s = specific gravity of grains; e = voids ratio, n = porosity, γ_t = in situ density.

The volumetric soil moisture profile of the saprolitic soil extracted from the trench, located behind Building B, is shown in Fig. 6. The results indicated volumetric water content around 25% on the surface and a gradual reduction

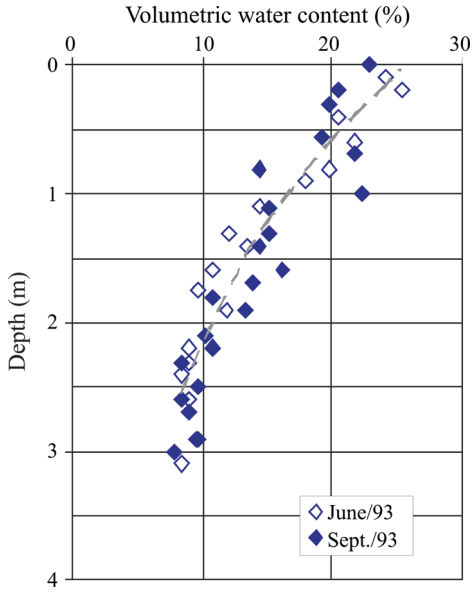

Figure 6 - Volumetric water content profiles of the saprolitic soil from the trench.

with depth. Below 2 m deep, this value is approximately constant and equal to 9%.

2.2 Shear strength parameters

Isotropically consolidated drained triaxial tests (CID) were performed on saturated 100 mm-diameter undisturbed samples of the saprolitic soil extracted from the trench. The specimens were molded with the xistosity plane inclined around 30° with the horizontal plane. The consolidation stress levels ranged from 25 to 200 kPa and the shearing velocity was 0.0122 mm/min. The triaxial chamber allowed for the use of internal devices for automatic measurement of axial and radial strains and volume changes (water and total volume). The variations of air volume were mechanically monitored by a bubble trap device (Aguilar, 1990).

Conventional direct shear tests were carried out on soil samples extracted from the slip surface. The saprolitic soil specimens were molded with the shearing plane parallel and perpendicular to the plane of xistosity. In spite of the apparent isotropic condition, the mature soil samples were also prepared according to perpendicular angles. The samples were initially saturated, prior to the consolidation stage, under normal stresses ranging from 22 to 135 kPa. The shearing velocity was 0.036 mm/min and the shear box was assembled with an opening of 0.5 mm between the two halves.

Figure 7 shows the shear strength test results of the saprolitic soil and Table 2 summarizes the mean values of strength parameters, with no influence of the shear plane angle with respect to the xistosity orientation having been observed. The results revealed a reasonable agreement between the direct shear and the triaxial tests of the saprolitic soil, despite the differences on soil characterization.

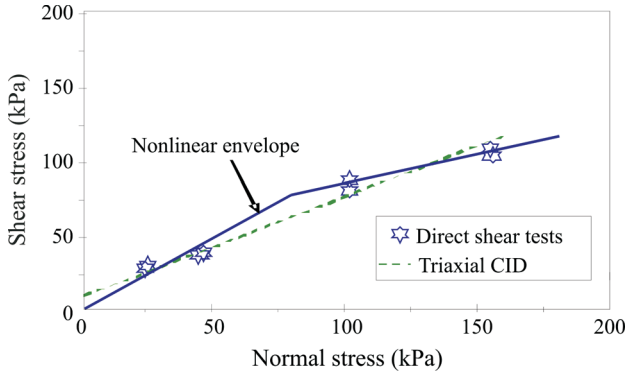

Figure 7 - Shear strength of saprolitic soil – saturated condition.

The Mohr-Coulomb strength envelope of the saprolitic soil could be fitted by a straight line with effective cohesion and friction angle equal to 13 kPa and 33°, respectively. However, due to the relatively high percentage of sand, it would be expected a null cohesion within the range of low confining stresses. For that reason, the Mohr-Coulomb strength envelope would better defined by a bi-linear curve that is also plotted in Fig. 7. The small thickness mature residual soil provided lower values of strength parameters as a result of a more intense weathering process.

The shear strength response of the residual soil under unsaturated condition was determined by direct shear tests with suction control. The tests were carried out on samples extracted from the slip surface, according to a multi stage technique (Ho & Fredlund, 1982), following the wetting path (Fonseca, 1991; Carrillo *et al.* 1994). Similarly to the saturated tests, specimens were molded with shearing planes parallel and perpendicular to the plane of xistosity. The samples were initially consolidated under a vertical stress of 50 kPa, and then submitted to decreasing suctions from 200 to 15 kPa (de Campos *et al.*, 1994). The shearing velocity was equal to 0.0366 mm/min.

The shear strength of unsaturated soils is based on the Mohr-Coulomb criterion and, according to Fredlund *et al.* (1978), can be expressed by:

$$\tau = c' + (u_a - u_w)\text{tg}\phi^b + (\sigma - u_a)\,\text{tg}\phi' \qquad (1)$$

where u_a and u_w are the pore air and pore water pressures, respectively, σ is the total normal stress; c' and ϕ' are effective strength parameters and ϕ^b is the angle indicating the rate of increase in shear strength relative to the matric suction. ϕ^b is equal to ϕ' at low matric suction, and decreases to a lower value at high matric suctions (Tekinsoy *et al.*, 2004).

Table 2 - Saturated strength parameters.

Test soil	Conventional direct shear test		Triaxial test
	Saprolitic soil	Mature soil	Saprolitic soil
c'(kPa)	14.6	4.8	9.6
ϕ'(°)	31.8	27.5	34.0

Notes: c' = effective cohesion, ϕ' = effective friction angle.

Figure 8 shows the shear strength results with respect to soil suction. Similar to the saturated soil response, no influence of xistosity plane on the soil strength was observed. The nonlinear relationship between the shear strength and soil suction was fitted by a bi-linear curve with $\phi^b = 33°$, for soil suction up to 115 kPa, and equal to 20°, for higher values. For low soil suctions values, the ϕ^b value was equivalent to ϕ'.

The similarity between ϕ^b and ϕ', for low values of matric suction, was also observed by Rahardjo *et al.* (1995) in triaxial tests on residual soils of Singapore. Following a drying path, the authors obtained ϕ^b equal to 26°, for matric suctions up to 400 kPa, which was equal to the soil effective friction angle ϕ'.

It is worth to note that the relatively high ϕ^b values revealed the strong influence of the matric suction on the shear strength; thus, any infiltration process promotes a substantial reduction of the shear strength.

2.3. Hydraulic parameters

The hydraulic conductivities profiles were obtained by laboratory tests on 100 mm-diameter samples and in the field by means of Guelph permeameter tests (Reynolds & Elrick, 1987). The results in Fig. 9 reveal a sharp decrease of the relative hydraulic conductivity (k/k_{sat}) with the increase of matric suction, within the first 3 m of the soil profile. Below this depth, the hydraulic conductivity parameters were considered constant.

Soil-water retention curves (SWCC) were obtained from the saprolitic soil samples from the slip surface, following drying and wetting paths. The results, shown in Fig. 10, indicated no significant deviation between the wetting and drying curves. Characterization of the saprolitic soil of the slip surface (Table 1) indicates that the saturated

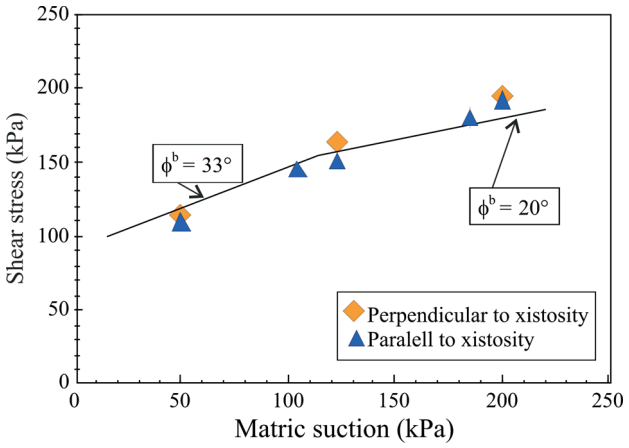

Figure 8 - Unsaturated strength envelope.

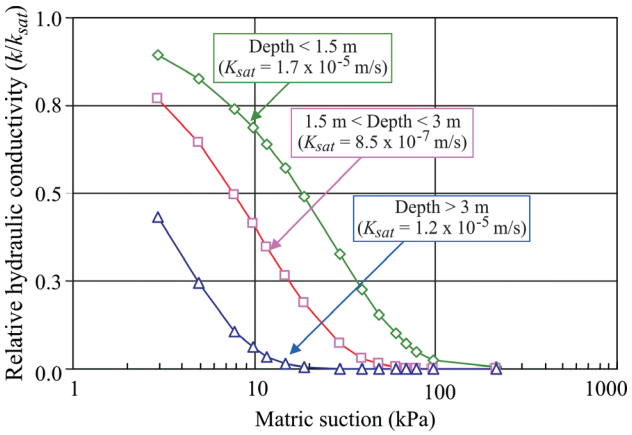

Figure 9 - Prescribed relative hydraulic conductivity curves.

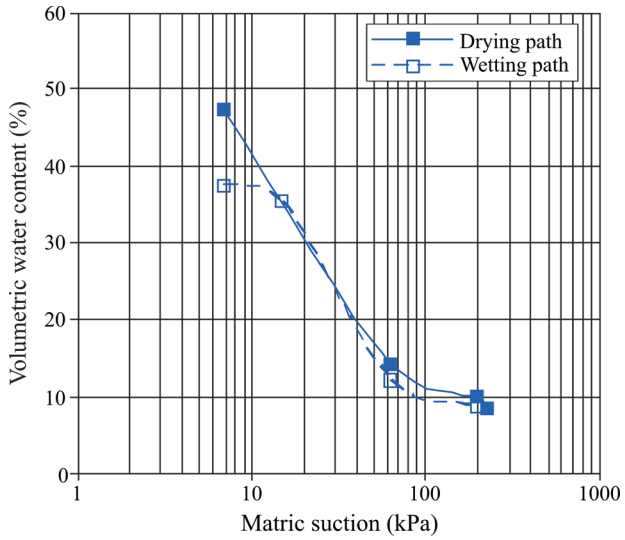

Figure 10 - Soil-water retention curve of the saprolitic soil from the slip surface.

volumetric water content ($\theta_s = n$ x S) is equal to 54%. However, the results suggests a lower value, around 40% that is mainly attributed to entrapped air effects. A more detailed description regarding the hydraulic parameters tests and data interpretation are presented in Gerscovich *et al.* (2006).

3. Transient Flow Simulations

The general equation that controls steady-unsteady state flow problems through 3-D saturated-unsaturated porous media, usually referred to as Richards' equation, may be written as:

$$\frac{\partial}{\partial x_i}\left[k_{ij}^s K_r \frac{\partial h_p}{\partial x_i} + k_{ij}^s K_r\right] = \left[C(\psi) + \frac{\theta(\psi)}{n} S_s\right]\frac{\partial h_p}{\partial t} \qquad (2)$$

where h_p is the pressure head, ψ is the matric suction, θ is the volumetric water content (V_w/V), k_{ij}^s is the tensor of hydraulic conductivity at saturation; K_r is the relative hydraulic conductivity, which is defined as the relationship between unsaturated and saturated hydraulic conductivities (k/k_{sat}); K_r is a scalar function of the degree of saturation ($K_r(S)$) that varies between 0 and 1; $C(\psi)$ is the volumetric water retention capacity ($\partial\theta/\partial\psi$), given by the tangent to the SWCC, n is the porosity and S_s is the coefficient of specific storage. S_s physically represents the volume of water that a unit volume of porous media releases from storage under a unit decline in hydraulic head (Freeze & Cherry, 1979). [$K_r\, k_{ij}^s$] represents the effect of the elevation head, since the equation is written in terms of pressure head.

A finite element program (FLOW3D) was specially developed (Gerscovich, 1994) to solve the general flow equation to evaluate flow processes that might have happened within the slope. Its code was derived from FPM500 finite element program (Taylor & Brown, 1967), which performs flow modeling within saturated soil media. The major modifications were based on the paper by Neuman (1973), in order to incorporate the unsaturated and transient conditions.

The mathematical development of the flow equation, built-in in the FLOW3D code, assumes that: i) flow is laminar and Darcian; ii) inertial forces, velocity heads, temperature gradients and chemical concentration gradients are all negligible; iii) soil is linearly elastic and isotropic; iv) hydraulic properties are not affected by volume changes; v) the air phase is continuous and always in connection with the constant, external atmospheric pressure; vi) the hysteretic behaviour of the SWCC is negligible; vii) the effect of soil compressibility on the storage of water under unsaturated conditions is quite small.

FLOW3D was tested for various steady and unsteady state flow conditions and geometries. 1D steady-state state response was evaluated by prescribing constant pressure heads at the boundaries of an unsaturated soil profile and comparing the results with the exact solution. 1D transient flow condition was evaluated by computing the volume of infiltrating water and comparing it with Buchanan *et al.* (1980) results. 2D steady state condition was evaluated by simulating flow infiltration through a homogeneous earth dam until the development of a phreatic surface that remained fixed and similar to Kozeny's solution. The 3D transient flow condition was evaluated by reproducing a 3D model experiment run by Akai *et al.* (1979). Detailed description of flow tests referrer to Gerscovich *et al.* (2006).

3.1. Slope geometry and boundary conditions

The 3D mesh comprised 1820 elements and 2436 nodes, as shown in Fig. 5b. The small thickness layer, located at the top of the slope (Fig. 5a), was disregarded in order to avoid excessive mesh discretization. It is worthwhile to mention that a 2D analysis of the center cross section of the slope revealed that the amount of the rainfall rate was

sufficient to fully saturate the small thickness layer. Consequently, its effect was indirectly incorporated by prescribing pressure heads at nodes located at the top boundary.

The lateral boundaries, bottom of the slope, as well as the slope toe were considered as impervious surfaces. At the slope surface, daily rainfall events were simulated by prescribing flow velocities at the surface nodes, according to the amounts registered at a pluviometric station, located 4 km away from the slope.

The time dependent characteristic of the transient flow through unsaturated soil requires the knowledge of the initial distribution of matric suction (or soil moisture), previous to the simulation period. Flow modeling assumed null suction at the slope surface and a progressive increase of matric suction with depth. Below 2 m-depth the soil suction was taken as constant and equal to 200 kPa. These values were assumed by evaluating both the water content profile of the saprolitic soil (Fig. 6) and the soil water retention curve (Fig. 10).

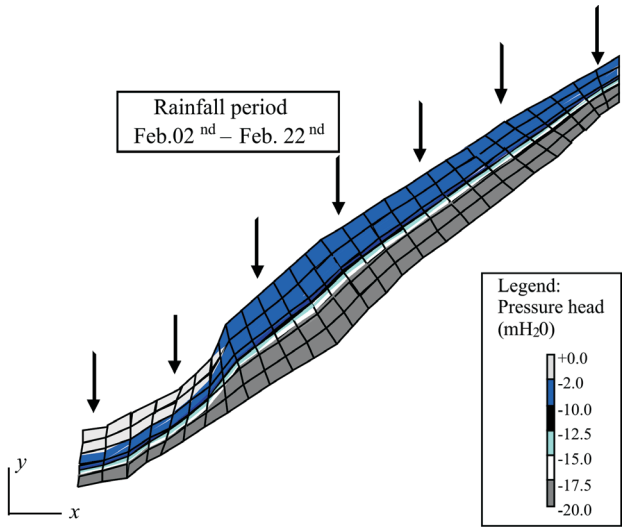

Figure 11 - Pressure head distribution at the central section of the slope - 3D Analysis (Gerscovich *et al.*, 2006).

3.2. Flow simulation results

Different scenarios of flow infiltration were analyzed in an attempt to reproduce the full saturation of the slope that was observed the day after the landslide, despite the inexistence of groundwater within the soil mass (Gerscovich *et al.*, 2006).

3.2.1. Case 1: Flow pattern predicted after 21 days of rainfall recorded in February, 1988

The influence of rainfall intensity was initially evaluated by analysing flow patterns considering a more intense rainfall that occurred few months before the landslide. In this period, the accumulated rainfall was approximately 2 times greater than the registered in November, 1988, prior to the landslide. The results, shown in Fig. 11, indicated slight changes in pressure head distributions, but no development of positive pore pressures within the soil slope. This pore-water pressure distribution is in disagreement to field observation after the landslide, since water was springing from the failure surface. This result, therefore, suggests that rain infiltration solely would not be sufficient to produce significant pore-water changes.

3.2.2. Case 2: Flow pattern predicted after 19 days of rainfall recorded in November, 1988, with an extra pressure head imposed at the top of the slope

The effect of disregarding the small thickness layer, located at the top of the slope, was evaluated by analysing its response to rain infiltration. Thus, a 2D flow analysis of this varying thickness layer (Fig. 5a) was carried out and revealed that 17 days of rainfall, prior to November 2nd (landslide day), could easily induce its complete saturation. In this study, the initial matric suction was set constant and equal to 10 kPa, the lower and bottom boundaries were impervious and null pressure heads were prescribed at the upper boundary.

The effect of the saturation of the upper layer was incorporated in the 3D numerical analysis by prescribing hydrostatic pressure heads at the top boundary nodes. In this study, flow velocities imposed at the nodes of the slope surface comprised 19 days of rain events, from October 19th to November 7th. Figure 12 presents the pressure head distribution predicted at the central section of the slope. Despite the generation of positive pore pressure at the upper zone, mainly due to the progress of a saturation front, this result still did not reproduce the saturation condition of the failure surface that was verified after the slide.

An additional numerical analysis was carried out in an attempt to evaluate if geometry changes of the slope, produced by the displacement of the soil mass after the landslide, could accelerate the progression of the saturation front. This hypothesis was tested by performing a 2D nu-

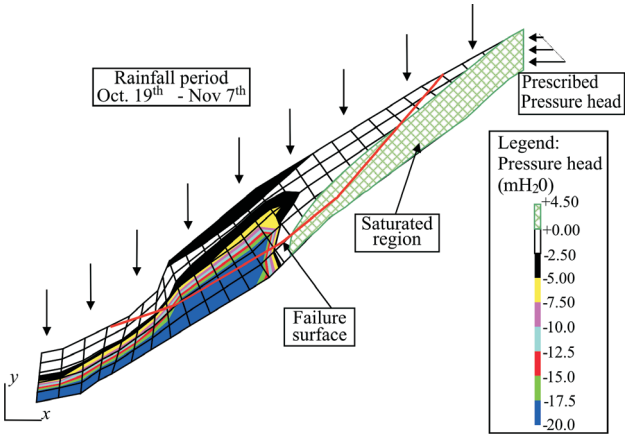

Figure 12 - Pressure head distribution in the central section of the slope; prescribed heads at the top of the slope - 3D Analysis (Gerscovich *et al.*, 2006).

merical simulation of the central section of the slope, including the small thickness layer, located at the top of the slope. In this analysis, a high value of saturated hydraulic conductivity (k_{sat} = 1) was used for the soil above the failure surface and null pressure heads were prescribed at the nodes at failure surface. The initial moisture conditions where equivalent to the ones predicted after 19 days of rain simulation (Fig. 12) and the remaining boundary conditions were unchanged. The results confirmed that few hours were sufficient to nearly cause a saturation of the whole soil mass and could be a feasible explanation for the saturation condition of the failure surface. However, it could not explain the landslide, since it was likely that large positive pore-water pressures would be required to reduce shear strength and cause the soil mass to fail.

3.2.3. Case 3: Flow pattern generated by a rainfall period of 5 days prior to the landslide and pressure heads prescribed at the top and at the base of the slope

Field investigations indicated the existence of a 4 to 10 m thick highly fractured rock layer at the transition of the sound rock and saprolitic soil. Maxima piezometers measured water levels restricted to this transition layer and confined to a small area.

The major role of the bedrock in generating high pore-water pressures have already been pointed out by other researchers (Dietrich *et al.*, 1986; Wilson, 1988; Vargas Jr. *et al.*, 1990). On the other hand, in the current engineering practice, it is very difficult not only to identify the existence of layers with high transmissivities but also to conceive an adequate mathematical model for this condition. Nevertheless, the influence of an eventual preferential flow through the fracture systems was roughly evaluated by prescribing positive pressure heads at 13 nodes, located along a transversal line of nodes at the base of the 3D mesh, as shown in Fig. 13. At each node, the magnitude of pressure head was equivalent to the vertical distance between the node coordinate and the highest point of the slope mesh. This simulation was carried out for a time of approximately 6 days, from November 2nd to November 7th. Boundary conditions and initial soil suction were similar to the ones used in the previous analysis. The numerical simulation (Fig. 13) showed that the whole soil mass nearly reached full saturation, with high levels of positive pore pressure been achieved and confirmed the major influence of water sources when they occur at the base of the slope.

4. Slope Stability Analyses

The stability analyses were carried out using the code SLOPE/W (GEO-SLOPE International Ltd – 2003), which allows for the computation of safety factors under in 2D conditions.

The slope profile consisted of a superficial mature residual soil and a variable thickness saprolitic soil layer. Due to the small thickness of the mature residual soil, this layer was disregarded and the stability analyses were carried out considering a homogeneous material.

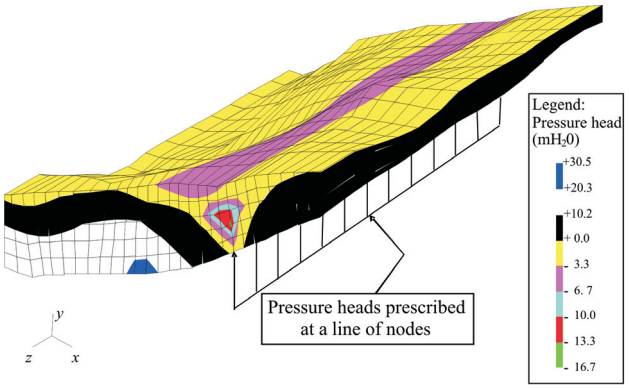

Figure 13 - Pressure head distribution – prescribed heads at the top and at the base of the slope- 3D Analysis (Gerscovich *et al.*,

The geotechnical parameters were obtained from laboratory tests and are listed in Table 3. The non-linearity of the effective strength envelope, obtained from Fig. 7, was adjusted by two straight lines crossing at a confining stress equal to 80 kPa. Due to limitations of the computer program, the unsaturated strength parameter (ϕ^b) was assumed constant and equal to the average value of the experimental results.

It is worthwhile to mention that the strength parameters correspond to peak values, as the stress-strain curves did not show any loss of strength for high strain levels.

The stability analyses were undertaken for the different scenarios of flow infiltration previously described. The pore-water pressure distributions at the central section of the slope were incorporated in the SLOPE/W program through a mesh of 46 nodes, as the program presents a limitation of the maximum number of nodes (50 nodes). The effect of pore air pressure was disregarded.

4.1. Case 1: Flow pattern predicted after 21 days of rainfall recorded in February, 1988

Figure 14 displays the set of results of Morgenstern & Price method for a slip surface similar to the one observed in situ (FS = 4.1) and for a potential failure surface derived

Table 3 - Geotechnical parameters.

Soil Parameter	Shear stress level (kPa)	
	≤ 80.0	> 80.0
γ_t (kN/m^3)	17.5	17.5
c' (kPa)	0	44.2
ϕ' (°)	43.7	22
ϕ_b (°)	25	25

Notes: ϕ^b = rate of increase in shear strength relative to the matric suction.

from center grid search (FS = 3.5). Both analyses provided high factors of safety and the potential failure surface showed an higher initiation point and a larger volume of the displaced soil mass.

Shear tests with unsaturated samples indicated a bilinear relationship between shear strength and matric suction and relatively high ϕ^b values. The influence of the matric suction on the safety factor was evaluated by performing analyses with $\phi^b = 0$. The factors of safety obtained were relatively high and equal to 1.53 and 1.67, for the circular search and field surfaces, respectively.

Stability analyses were also carried out in order to identify the likely range of shear strength parameters that would result in a FS close to 1. The smallest factors of safety (FS = 1.13 and 1.17, for the circular search and field surfaces, respectively) were computed by disregarding the influence of the matric suction and using the effective strength parameters obtained in the saturated CID tests.

It is worthwhile to emphasize that the analyses were carried out considering a plane strain condition. The 3D feature of the landslide would undoubtedly provide higher factors of safety.

The computed FS revealed that an ordinary amount of rain infiltration would not be sufficient to trigger the slope failure. These results are in accordance to the conclusions derived from the numerical simulations of rain infiltration, since it did not reproduce the saturated condition of the failure surface.

4.2. Case 2: Flow pattern predicted after 19 days of rainfall recorded in November, 1988, with an extra pressure head imposed at the top of the slope

The small thickness layer at the top of the slope (Fig. 5a) was disregarded to improve 3D mesh discretization. However, full saturation of this region could actually have happened and imposed an additional boundary condition. 2D flow simulation of this layer (Fig. 5a) subjected to 17 days of rain infiltration, prior to the landslide day, resulted in complete saturation of this soil.

This alternative was taken in account in the 3D flow analysis by prescribing hydrostatic pressure heads at the nodes located at the upper boundary of the mesh. The 3D numerical flow simulation revealed a localized positive pore pressure generation at the upper zone, mainly due to the progress of a saturation front. At the failure surface the soil mass remained unsaturated and, therefore, did not reproduce field condition.

Stability analyses, corresponding to the observed field surface and potential failure surface provided values of FS higher than 1.5, as shown in Fig. 15. Thus existence of a water source at the top of the slope promoted an increase of the pore water pressure mesh, which was definitely not sufficient to trigger the landslide.

4.3. Case 3: Flow pattern generated by a rainfall period of 5 days prior to the landslide and pressure heads prescribed at the top and at the base of the slope

The results of the 3D numerical simulations of different flow scenarios pointed out that, besides rain infiltration, other mechanisms might played a major role on the slope hydrological pattern. Field investigations have indicated the existence of a highly fractured rock layer at the transition between the saprolitic soil and the sound rock. This layer was, therefore, incorporated in the flow analyses assuming that preferential flow paths through the fractures could act as deep water sources at different positions of the base of the slope. The 3D flow simulation of 6 days of rain infiltration resulted in an almost full saturation condition of the whole soil slope (Gerscovich *et al.*, 2006). The loss of soil suction followed by generation of positive pore pressure appeared as an ideal condition for the landslide. In fact,

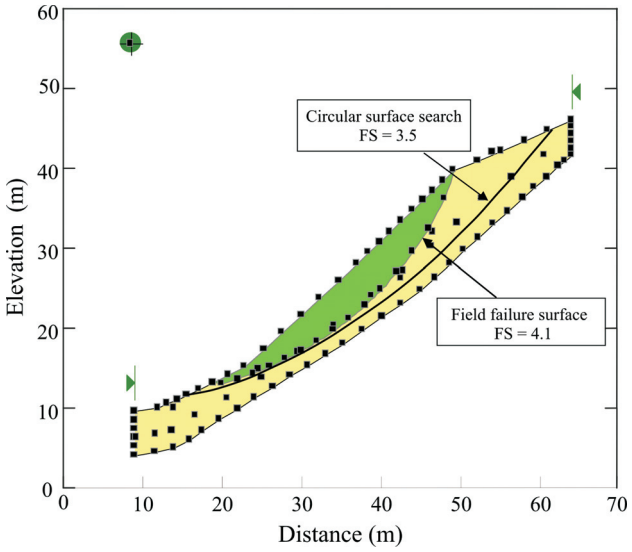

Figure 14 - Failure surfaces and Factors of Safety – Case 1.

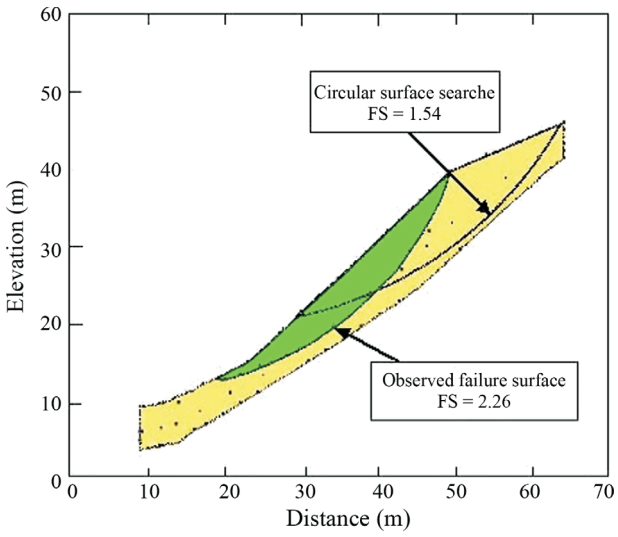

Figure 15 - Failure surfaces and Factors of Safety – Case 2.

the use of a pore water pressure mesh that reproduced this scenario, resulted in FS values less than 1 (Fig. 16) and, confirmed the assumption that the rainfall amount itself would not sufficient to justify the soil failure.

5. Conclusions

In an attempt to identify the triggering mechanism of the deep-seated slide of a slope, in Rio de Janeiro, Brazil, a comprehensive experimental investigation, 3D numerical flow analyses and stability analyses were undertaken. The landslide occurred after a rainfall period and despite the unsaturated soil condition, on the following day and even one week after the slide full saturation of the failure surface, with groundwater sprouting at its upper region, was clearly observed.

The slope consisted of a varying thickness layer of a residual soil overlying a gneissic rock that outcropped at the upper and left sides of the landslide boundary. The transition between the sound rock and the saprolitic soil was densely fractured.

A 3D-FEM transient/unsaturated flow program was used to simulate various flow scenarios in an attempt to assess the suitable condition that could promote the generation of positive pore water pressure within the slope. The flow analyses not only considered different rainfall rates, but also the influence of the soil saturation at the upper part of the slope, as a result of the malfunction of a surface drainage system, and an eventual development of a preferential flow paths through the fractured rock layer. The studies revealed that the existence of a water source at the base of the slope appeared to be the only feasible scenario that could explain the hydrological condition after the landslide.

A series of shear strength laboratory tests, carried out under saturated and unsaturated soil conditions revealed that a single strength envelope could be used for the entire slope. These strength parameter were used with the different pore water pressure meshes, which were conceived from the results of flow simulations.

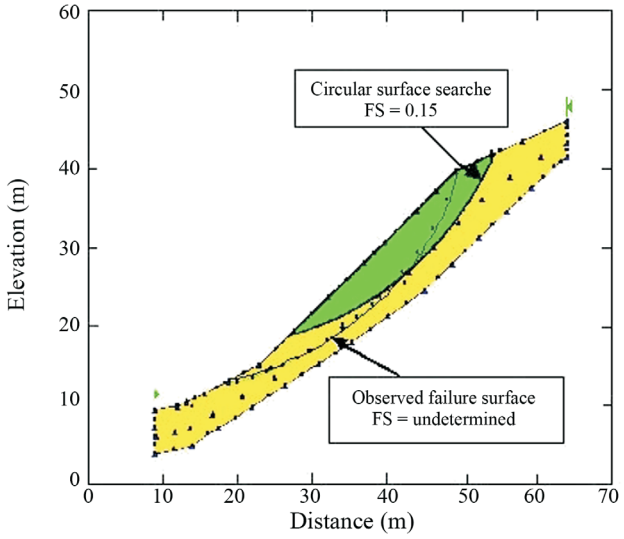

Figure 16 - Failure surfaces and Factors of Safety – Case 3.

The stability analyses of the central section of the landslide, indicated high values of FS, except for the most severe flow condition that assumed water sources at different positions of the failure surface; *i.e.*, the rainfall amount that reached slope surface before the landslide was not sufficient to trigger slope failure. These slope stability results agreed with the 3D flow simulations, since full saturation of the failure surface was only predicted if mechanisms other than rain infiltration were prescribed.

The authors consider that the main conclusion of this study is that, despite the development of experimental and numerical techniques to address the behavior of unsaturated soils, the understanding of the complex phenomenon of rainstorm-induced landslides is still a challenge among geotechnical engineers. Besides, except for extreme and unpredictable rainfall amounts, landslides are probably triggered by a combination of mechanisms. Therefore, geotechnical engineers must call attention to the complexity of landslides in unsaturated residual soils, and always try to answer a simple question that many times arises: why the landslide did not occur during a more intense event or why it did not occur few meters away?

Acknowledgments

The authors acknowledge the financial support from the International Development Center (IDRC), Canada, the National Council for Research (CNPq) and the Rio de Janeiro Research Support Agency (FAPERJ), Brazil. The authors are also grateful to all graduate students that participated in this research project.

References

Akai, K.; Ohnishi, Y. & Nishigaki, M. (1979) Finite element analysis of three-dimensional flow in saturated-unsaturated soils. Proc. 3rd Int. Conf. Numerical Methods in Geomechanics, Aachen, pp. 227-239.

Au, S.W.C. (1998) Rain-induced slope instability in Hong Kong. Engineering Geology, v. 51:1, p. 1-36.

Brand, E.W. (1985) Geotechnical engineering in tropical residual soils. Proc. 1st Int. Conf. on Geomechanics in Tropical Lateritic and Saprolitic Soils, Brasília, v. 3, pp. 23-100.

Buchanan, P.; Savigny, K.W. & de Vries, J. (1980) A method for modeling water tables at debris avalanche headscarps. Journal of Hydrology, 113, p. 61-68.

Capra, L.; Lugo-Hubp, J. & Borselli, L. (2003) Mass movements in tropical volcanic terrains: the case of Teziulán (Mexico). Engineering Geology, 69, p. 359-379.

Carrillo, C.W.; Fonseca, E.C. & de Campos, T.M.P. (1994) Suction controlled direct shear device. Proc. 2nd Symp. on Unsaturated Soils, Recife, pp. 67-78 .

Costa Nunes, A.J.; Couto Fonseca, A.M.M.C.; Couto Fonseca, de M.; Fernandes, C.E. & Craizer, W. (1989) In-

tense rainstorm and ground slides. Proc. 12th Int. Conf. Soil Mech. and Found. Engn, v. 3, pp. 1627-1630.

de Campos, T.M.; Andrade, M.H.N.; Gerscovich, D.M.S. & Vargas Jr., E.A. (1994) Analysis of the failure of an unsaturated gneissic residual soil slope in Rio de Janeiro, Brazil. Proc. 1st. Pan Am. Symp. of Landslides, Guayaquil, v. 1, pp. 201-213.

Dietrich, W.E.; Wilson, C.J. & Reneau, S.L. (1986) Hollows, colluvium, and landslides in soil mantled landscapes. A.D. Abrahams (ed) Hillslope Processes, Allen & Unwin Ltd, pp. 361-368.

Fonseca, E.C. (1991) Ensaio de Cisalhamento Direto com Sucção Controlada em Solos Não Saturados. MSc. Thesis. Departamento de Engenharia Civil, Universidade Católica do Rio de Janeiro.

Fredlund, D.G.; Morgenstern, N.R. & Widger, R.A. (1978) The shear strength of unsaturated soils. Canadian Geotechnical Jour., 15, p. 228-232.

Freeze, R.A. & Cherry, J.A. (1979) Groundwater. Prentice-Hall, Inc., Englewood Cliffs.

Gasmo, J.M.; Rahardjo, H. & Leong, E.C. (2000) Infiltration effect son stability of a residual soil slope. Computers and Geotechnics, 26, p. 145-165.

GEO-SLOPE International Ltd. (2001). SLOPE/W for slope stability analysis, version 5.0.

Gerscovich, D.M.S. (1994) Fluxo em Meios Porosos Saturados e Não Saturados Modelagem Numérica com Aplicações ao Estudo da Estabilidade de Encostas do Rio de Janeiro. DSc. Thesis, Departamento de Engenharia Civil, Universidade Católica do Rio de Janeiro.

Gerscovich D.M.S.; de Campos T.P.P. & Vargas Jr., E.A. (2006) On the evaluation of unsaturated flow in a residual soil slope in Rio de Janeiro Brazil. Engineering Geology, 88, p. 23-40.

Ho, D.Y.F & Fredlund, D.G. (1982) The increase in shear strength due to soil suction for two Hong Kong soils. Proc. ASCE Geotech. Conf. on Engn. Construction in Tropical and Residual Soils, Honolulu, pp. 263-295.

Kim, J.; Jeong, S.; Park, S. & Sharma, J. (2004) Influence of rainfall-induced wetting on the stability off slopes in weathered soils. Engineering Geology, 75, p. 251-262.

Neuman, S.P. (1973) Saturated-unsaturated seepage by finite elements. Journal of Hydraulics Division, 99 (HY12), p. 2233-2250.

Rahardjo, H.; Lim, T.T.; Chang, M.F. & Fredlund, D.G. (1995) Shear strength characteristics of a residual soil. Canadian Geotechnical Journal, 32, p. 60-77.

Reynolds, W.D. & Elrick, D.E. (1987) A laboratory and numerical assessment of the Guelph permeameter method. Soil Science, v. 144:4, p. 282-292.

Taylor, M.E. & Brown, C.B. (1967) Darcy's flow solution with free surface. Journal of Hydraulics Division, HY2, p. 25-33.

Tekinsoy, M.A.; Kayadelen, C.; Keskin, M.S. & Soylemez M. (2004) An equation for predicting shear strength envelope with respect to matric suction. Computers and Geotechnics, v. 31, p. 589-593.

Vargas Jr., E.A.; Costa Filho, L.M. & Prado Campos, L.E. (1986) A study of the relationship between stability of the slopes in residual soils and rain intensity. Proc. Int. Symp. on Environmental Geotechnology, pp. 491-500.

Vargas Jr., E.A.; Velloso, R.C.; de Campos, T.M.P. & Costa Filho, L.M. (1990) Saturated-unsaturated analysis of water flow in slopes of Rio de Janeiro, Brazil. Computers and Geotechnics, v. 10:3, p. 247-261.

Wang, G. & Sassa, K. (2003) Pore-pressure generation and movement of rainfall-induced landslides: effects of grain size and fine-particle content. Engineering Geology, 69, p. 109-125.

Wilson, C.J. (1988) Runoff and Pore Pressure Development in Hollows. PhD Thesis, Department of earth and Planetary Science, California University, Berkeley.

Wolle, C.M. & Hachich, W. (1989) Rain-induced landslides in south-eastern Brazil. Proc. 12th Int. Conf. Soil Mech. and Found. Engn., v. 3, p. 1639-1644.

List of Symbols

G_s: specific gravity of grains
S: degree of saturation
n: porosity
e: voids ratio
ψ: matric suction
γ_i: in situ density
θ: volumetric water content
ω: water content (in weight)
V_w: volume of water
V: total volume
ω_{LL}: liquid limit
ω_{LP}: plasticity limit
c': effective cohesion
ϕ': effective friction angle
ϕ^b: rate of increase in shear strength relative to the matric suction
u_a: pore air pressure
u_w: pore water pressure
$(u_a - u_w)$: matric soil suction